INORGANIC CHEMISTRY FRONTIERS

RESEARCH ARTICLE

View Article Online
View Journal | View Issue

Cite this: *Inorg. Chem. Front.*, 2024, **11**, 409

Molecular insight into intrinsic-trap-mediated emission from atomically precise copper-based chalcogenide models†

Yi-Lei Xu,‡[a] Yayun Ding,‡[b] Lin-Mei Zhang,[a] Hao Ma,[a] Jia-Xing Liu,[a] Jiaxu Zhang,[b] Rui Zhou,[a,c] Dong-Sheng Li,[d] Shang-Fu Yuan *[a] and Tao Wu *[a,b]

Luminescent Cu-doped semiconductor nanocrystals have long played a pivotal role in the advancement of lighting and display technologies. The luminescence observed in colloidal copper-based I–III–VI nanocrystals is attributed to defect emission arising from donor–acceptor pair recombination of excited charge carriers. However, a detailed atomic-level exploration of how distinct chemical components precisely influence the defect position has remained challenging, primarily due to inherent local structural imprecision of the traditional I–III–VI nanocrystals. In this study, we have prepared a set of copper-containing I–III–VI metal chalcogenide nanoclusters, **1-CuInS**, **1-CuGaS**, and **2-CuGaS**, serving as unique models to address the aforementioned issues. Interestingly, despite possessing an identical crystalline structure, **1-CuInS** and **1-CuGaS** exhibit significantly different photoluminescence behaviors. For comparsion, **1-CuGaS** and **2-CuGaS**, which share the same second building units but differ in structural configuration, demonstrate similar luminescence performance. More importantly, we found that the green emission observed in **1-CuInS** likely stems from the radiative recombination of electrons migrating from shallow delocalized traps to copper-localized holes. In contrast, the red emission observed in both **1-CuGaS** and **2-CuGaS** is presumably due to the recombination of electrons originating from deeply localized traps with copper-localized holes. This disparity in trap sites appears to be highly dependent on the presence of trivalent metal ions (In^{3+} and Ga^{3+}) within the clusters, and the hypothesis is further substantiated through photoluminescence characterization of **1-CuInGaS** containing both In^{3+} and Ga^{3+} ions simultaneously. Furthermore, we have explored the impact of introducing Cd ions into **1-CuInS**, which can alter the position of shallow delocalized traps and thereby fine-tune the luminescence properties. Our findings shed light on the intricate interplay of chemical composition and defect states in copper-containing I–III–VI nanoclusters, offering valuable insights into the optoelectronic properties of copper-based semiconductor nanocrystals.

Received 17th October 2023,
Accepted 17th November 2023

DOI: 10.1039/d3qi02132g

rsc.li/frontiers-inorganic

Introduction

Metal chalcogenide semiconductor nanocrystals, also referred to as quantum dots (QDs), have captivated the scientific and technological community over the past few decades due to their intriguing photoluminescence (PL) properties.[1–5] Among these, copper-based I–III–VI nanocrystals have garnered particular interest, attributable to their photophysical characteristics, such as optically activated copper midgap states, tuneable photoluminescence (PL) behavior across the visible and near-infrared (NIR) spectral range, and a composition free from toxic elements such as Cd or Pb,[6–10] making them promising substitutes for most II–VI and IV–VI nanocrystals. Consequently, these nanocrystals hold potential applications in light-emitting diodes, nonlinear optics, and biomedical labeling.[11–14] In this regard, extensive research efforts have

[a]*College of Chemistry and Materials Science, Guangdong Provincial Key Laboratory of Functional Supramolecular Coordination Materials and Applications, Jinan University, Guangzhou 510632, China. E-mail: sfyuan@jnu.edu.cn, wutao@jnu.edu.cn*
[b]*College of Chemistry, Chemical Engineering and Materials Science, Soochow University, Suzhou, Jiangsu 215123, China*
[c]*Department of Developmental and Regenerative Biology, Jinan University, Guangzhou 510632, China*
[d]*College of Materials and Chemical Engineering, Hubei Provincial Collaborative Innovation Centre for New Energy Microgrid, Key Laboratory of Inorganic Nonmetallic Crystalline and Energy Conversion Materials, China Three Gorges University, Yichang 443002, China*

†Electronic supplementary information (ESI) available: Experimental details, physical measurements, and additional figures and tables. CCDC 2062543 for **1-CuInS**, 2062544 for **1-CuGaS** and 2062545 for **2-CuGaS**. For ESI and crystallographic data in CIF or other electronic format see DOI: https://doi.org/10.1039/d3qi02132g

‡These authors contributed equally to this work.

been dedicated to unfolding the luminescence mechanisms and investigating the factors that influence the properties of copper-based I–III–VI nanocrystals, with the aim of enhancing their optoelectronic performance and further applications.

In general, the luminescence observed in copper-based I–III–VI nanocrystals serves as a quintessential example of the donor–acceptor pair (DAP) emission mechanism, which is related to the recombination of excitons, where electrons located in inherent defect sites situated below the conduction band act as donor states, and holes trapped in Cu vacancy (V_{Cu}).[2,6,15,16] Previous efforts have demonstrated that both the composition and surface structure of these nanocrystals play a crucial role in determining the location and types of intrinsic defects, exerting a significant influence on the emission performance.[15,17,18] However, despite special emphasis has been placed on understanding the defect-induced luminescence of I–III–VI nanocrystals, the correlations between chemical components and defect positions have yet to be systematically explored, primarily due to the inherent uncertainties of the atomic position in typical I–III–VI nanocrystals. Furthermore, the size inhomogeneity of QDs also presents challenges in elucidating the mechanism behind defect-mediated emission.

In this aspect, metal chalcogenide supertetrahedral nanoclusters (Tn, *n* indicates the number of metal layers along the edge of the tetrahedron) with precisely defined compositions and uniform sizes could serve as excellent model system to solve the above issue (Scheme 1).[19–29] In previous study, Mn-related emission have been studied in detail in Mn based II–III–VI supertetrahedral nanoclusters. For instance, our investigations have delved into the role of dipole–dipole interactions directed by Mn–Mn distances in controlling Mn-related emissions through the examination of three structurally well-defined Mn-based II–III–VI supertetrahedral nanoclusters (MCOF-5, MCOF-6, and MCOF-7).[30] In contrast, there has been a relative scarcity of investigation into the luminescence mechanism of copper-related emission from Cu-based I–III–VI supertetrahedral nanoclusters.[31–34]

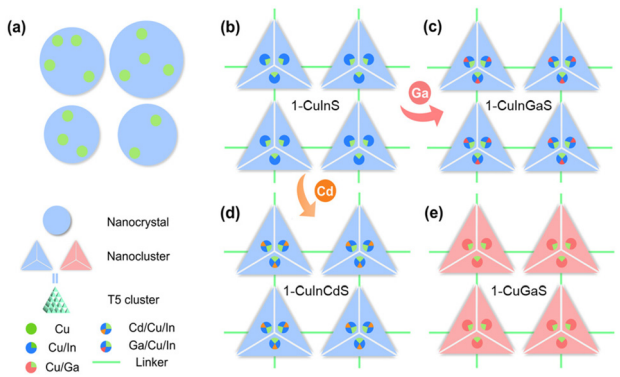

Scheme 1 (a) Cu-based classical I–III–VI nanocrystals with imprecise sites of Cu ions and inhomogeneous particle sizes. Copper-based chalcogenide supertetrahedral nanoclusters including (b) **1-CuInS**, (c) **1-CuInGaS**, (d) **1-CuInCdS**, and (e) **1/2-CuGaS** with relatively precise sites of Cu ions and homogeneous cluster size.

Herein, a series of copper-based I–III–VI metal chalcogenides (**1-CuInS**, **1-CuGaS**, and **2-CuGaS**) were synthesized and their photoluminescence behaviors were found strongly depend on the specific components present. Specifically, both **1-CuInS** and **1-CuGaS** are constructed by the assembly of supertetrahedral T5-$Cu_5M_{30}S_{56}$ clusters which are linked by [MSb_4S_{10}] units (M = In for **1-CuInS** and M = Ga for **1-CuGaS**). In contrast, **2-CuGaS** adopts the same second building units (SBUs) as **1-CuGaS** but utilizes [SbS_3] units as linkers. Interestingly, at room temperature, **1-CuInS** emits green luminescence, whereas **1-CuGaS** and **2-CuGaS** only emit red luminescence at low temperatures. Temperature-dependent PL and PL decay dynamics analysis indicated that the green emission originates from shallow delocalized traps while the red emission arises from deep localized traps, and both resulting in radiative recombination with Cu vacancy acceptor. Additionally, the emission of **1-CuInS** could be finely tuned through doping cadmium ions in the parent clusters due to the modulating of the position of the shallow delocalized traps.

Results and discussion

Synthesis and characterization of 1-CuInS, 1-CuGaS, and 2-CuGaS

Crystalline samples discussed here were synthesized *via* a similar solvothermal method with different types of protonated organic amines as templates (see the ESI† for more details). Their crystalline structures were determined by single-crystal X-ray diffraction (SCXRD), and compositions were further confirmed by energy dispersive X-ray spectroscopy (EDS) and elemental analysis (EA) (Fig. S1–S3†). In addition, the phase purity and thermal stability of the as-synthesized samples were characterized by powder X-ray diffraction (PXRD) (Fig. S4–S6†) and thermal gravimetric analysis (TGA) (Fig. S7–S9†), respectively. Furthermore, X-ray photoelectron spectroscopy (XPS) confirmed that Cu atoms in all the three structures were monovalent (Fig. S10†).

SCXRD analysis indicates that **1-CuInS** and **1-CuGaS** crystallize in the same space group tetragonal $I4_1/a$ with very similar unit cell parameters while **2-CuGaS** crystallizes in the hexagonal space group $P6_3/m$ (Table S1†). The structures of **1-CuInS** and **1-CuGaS** are isomorphic, characterized by the assembly of supertetrahedral T5-$Cu_5M_{30}S_{56}$ clusters linked by [MSb_4S_{10}] units (M = In for **1-CuInS** and M = Ga for **1-CuGaS**) (Fig. 1a and b). At the center of the linker is the tetrahedral [MS_4] unit, which is further connected with four trigonal-pyramidal [SbS_3] units through corner sulfurs, resulting in the formation of a [MSb_4S_{10}] unit with windmill shape when viewed along the *c* axis (Fig. S11†). Each [MSb_4S_{10}] unit joins for four T5-$Cu_5M_{30}S_{56}$ cluster through corner-shared μ-S^{2-} and *vice versa*, creating a double-interpenetrated framework with diamond topology (Fig. S12a, S12b, and S13a†). For **2-CuGaS**, it pos-

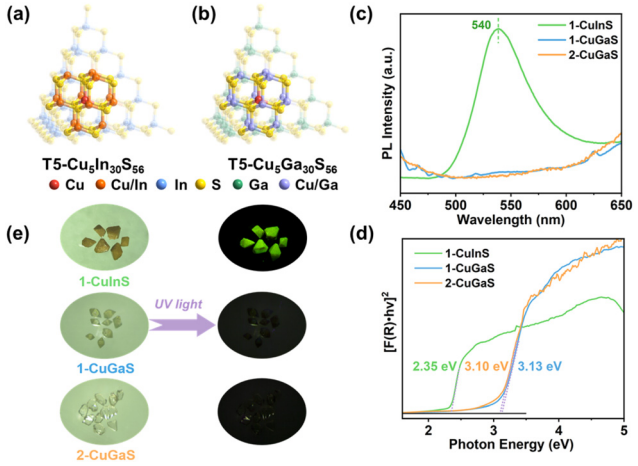

Fig. 1 (a) Supertetrahedral $[Cu_5In_{30}S_{56}]$ cluster in **1-CuInS**. (b) Supertetrahedral $[Cu_5Ga_{30}S_{56}]$ clusters in **1-CuGaS**. (c) RT PL spectra of **1-CuInS**, **1-CuGaS**, and **2-CuGaS**. (d) Tauc plots of **1-CuInS**, **1-CuGaS**, and **2-CuGaS** derived from UV-Vis DRS. (e) The optical images of pristine crystals with and without irradiation of an UV lamp.

sesses the same second building units (SBUs) as **1-CuGaS** but with different linkers (Fig. 1b). Each $[SbS_3]$ linker in **2-CuGaS** bridges three T5-$Cu_5Ga_{30}S_{56}$ clusters and each T5-$Cu_5Ga_{30}S_{56}$ connects to four neighboring clusters by four $[SbS_3]$ units, which give rise to a two-dimensional honeycomb (hcb) net (Fig. S12c and S13b†).

Interestingly, despite bearing similar supertetrahedral T5-$Cu_5M_{30}S_{56}$ units, the three crystalline samples exhibit distinct photoluminescence properties. As illustrated in Fig. 1c, **1-CuInS** displayed a strong green emission peak at 540 nm with a broad full width at half-maximum (fwhm) of 0.242 eV under excitation of 420 nm at room-temperature (RT). However, the luminescence of **1-CuGaS** and **2-CuGaS** was negligible at RT (Fig. 1e). The observation of green emission in **1-CuInS** is reminiscent of the so-called copper "green" ("G-Cu") luminescence in many Cu^+-doped semiconductors with different compositions.[35] In addition, the UV-Vis diffuse-reflectance spectra of the three samples were measured. As indicated in Fig. 1d, **1-CuInS**, **1-CuGaS** and **2-CuGaS** were semiconductors, and their corresponding band gaps were detected to be 2.35 eV, 3.13 eV, and 3.10 eV, respectively. Ultraviolet photoemission spectroscopy (UPS) measurements revealed that they had a similar valence band position (5.14 eV for **1-CuInS**; 5.10 eV for **1-CuGaS**, and 4.97 eV for **2-CuGaS**) (Fig. S14a†). Notably, **1-CuInS** and **1-CuGaS** displayed conspicuously different photoluminescence performances although they possessed identical frameworks and with different chemical compositions in the T5 SBUs. Conversely, **1-CuGaS** and **2-CuGaS** with the same SBUs both exhibited no emission at RT. These findings have spurred our interest for further research.

Temperature-dependent PL property of 1-CuInS, 1-CuGaS, and 2-CuGaS

To uncover the mechanism behind Cu-related emission, temperature-dependent PL spectra were performed on these crystalline samples. Fig. 2a displays the temperature-dependent PL spectra of **1-CuInS**. Upon cooling from 308 to 68 K, the emission peak wavelength (λ_{max}) gradually blue-shifted from 541 nm to 518 nm, accompanied by a slight reduction in the PL fwhm from 0.231 eV to 0.204 eV (Fig. 2b). Meanwhile, the maximum excitation wavelength shifted from 504 nm to 486 nm according to PLE spectra (Fig. S15a†). Furthermore, we obtained the integrated PL data in Fig. 2a to illustrate the relationship between PL intensity and temperatures, as demonstrated in Fig. 2c. As the temperature decreased, the PL intensity of **1-CuInS** increased non-monotonically. The initial increase in PL intensity from 308 to 158 K was mainly due to the suppression of non-radiative recombination pathways. However, the following decrease in PL intensity from 158 to 68 K is rather anomalous. The emission peak wavelength blue-shifts as the temperature decreases, ruling out the possibility of thermally activated delayed luminescence but suggesting negative thermal quenching (NTQ). NTO is an occasional phenomenon, which has been observed previously in defect emission.[36] It is generally been explained by thermally activated carrier transfer from lower- to higher-energy emissive electron traps. Fig. 2d plots the energy of the Cu-related emission peak *versus* temperature. The orange solid line represents the fitting of these temperature-dependent peak energies to the Varshni equation:

$$E_g = E_0 - \alpha T^2/(T + \beta)$$

where E_g is the energy gap in semiconductors, E_0 represents its value at 0 K, and α, β are constants.[16,37,38] The values were found [E_0 = 2.41 eV, α = (10.1 ± 1.98) × 10^{-4} eV K^{-1}, β = (5.58 ± 1.73) × 10^2 K] with R^2 equal to 0.999. The good agreement provided strong support for the associations between the copper-

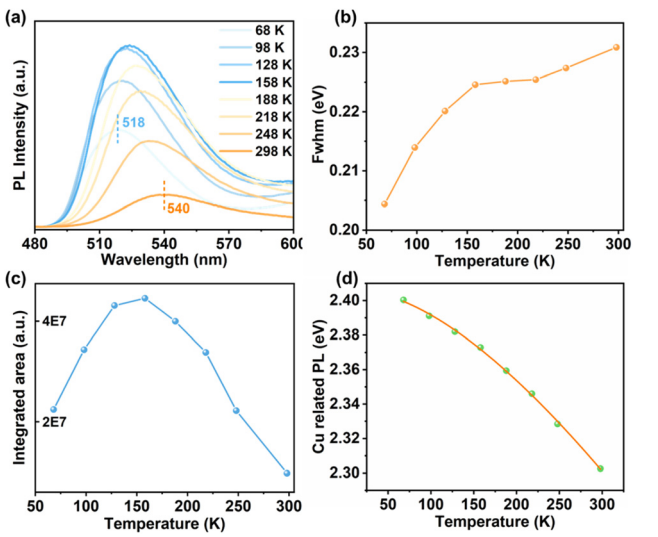

Fig. 2 Temperature-dependent PL properties of **1-CuInS**: (a) PL spectra under different temperatures. (b) Fwhm of the Cu-related green emission. (c) PL-integrated areas of different emission. (d) Plot of the energies of PL peaks *versus* temperature. The orange solid line represents fits of the data to the Varshni equation.

related PL of **1-CuInS** and the shallow delocalized traps, which vary with the position of the conduction band. A similar model has been proposed for bulk ZnS : Cu,[39] where the green emission originates from shallow delocalised traps, and the slight red shift of this emission was correlated with the shift of the conduction band to lower energies with increasing temperature.

Unexpectedly, although **1-CuGaS** and **2-CuGaS** exhibited almost no emission at RT, both were able to emit Cu^{+}-related red luminescence at lower temperatures. When cooling from 248 K to 68 K, the emission peak of **1-CuGaS** gradually redshifted from 621 nm to 643 nm and the emission intensity was remarkably increased (Fig. 3a). Notably, the maximum excitation wavelength showed negligible shifts during this process (Fig. S15b†). Similarly, the temperature-dependent PLE spectra of **2-CuGaS** demonstrated that the maximum excitation wavelength remained unchanged as the temperature decreased (Fig. S15c†). Also, **2-CuGaS** exhibited a similar redshift of emission peak and an increase in emission intensity with decreasing temperature (Fig. 3b). It is worth noting that, in comparison to **1-CuInS**, both **1-CuGaS** and **2-CuGaS** have larger optical band gaps and emit longer wavelength emissions, resulting in a larger Stokes shift. The redshift of the emission peak with the decrease of temperature in **1-CuGaS** and **2-CuGaS** suggests that the radiative recombination is less associated with shallow delocalised traps and could be explained by processes related to deeply-localized-traps. In such a situation, the excited state occupies lower vibration levels with temperature decreasing, leading to the redshift of the emission spectra.[35] Moreover, as depicted in Fig. 3c and d, the change of PL fwhm with temperature in **1-CuGaS** and **2-CuGaS** was comparable but much greater than that in **1-CuInS**. In all, the emission peak of **1-CuInS** shifted to higher energies with a decrease in temperature, accompanied by a slight reduction of half-widths. In contrast, the emission peaks of **1-CuGaS** and **2-CuGaS** shifted towards lower energies as the temperature decreased and half-widths of the spectra reduced significantly. Such differences in PL properties have been documented in cases involving different traps inducing copper-related emissions in Cu-based QDs.[35,40] More importantly, it is reasonable to conclude that the position of trap sites is closely related to the local surroundings (In^{3+} and Ga^{3+} ions) rather than the structural patterning modes of these structures.

PL decay dynamics of 1-CuInS, 1-CuGaS and 2-CuGaS

To investigate the origin of the green and red emissions in more detail, temperature-dependent excited-state lifetime of **1-CuInS**, **1-CuGaS**, and **2-CuGaS** were also recorded. As the temperature decreased, the PL decay time of **1-CuInS** increased from 128 ns at 298 K to 7.2 μs at 68 K, which was ascribed to the decrement of non-radiative pathways (Fig. 4a and b; Tables S2 and S3†). In comparison, **1-CuGaS** and **2-CuGaS** exhibited significantly longer decay lifetimes. These values reached approximately 158 μs for **1-CuGaS** and 214 μs for **2-CuGaS** at 68 K (Fig. 4c, d, and S16; Tables S4 and S5†). Normally, the lifetime of band edge emission in various semiconductor nanocrystals falls in the range of one to a few tens of nanoseconds, which is not the case in the present work. These indicate that the emission of all the three samples is expected to originate from dopant related channels, similar to many Cu-doped nanocrystals.[41] In addition, the literature suggests that the formation of long-lived photogenerated states in copper-doped nanocrystals, lasting from tens to hundreds of microseconds, is presumably associated with carrier localization at deep localised traps.[35] Wherein, the shallow-delocalized traps of **1-CuInS** and the deep-localized traps of **1-CuGaS** and **2-CuGaS** could also be reasonably explained. Furthermore, the gradual decrease in the average lifetime of both crystals with

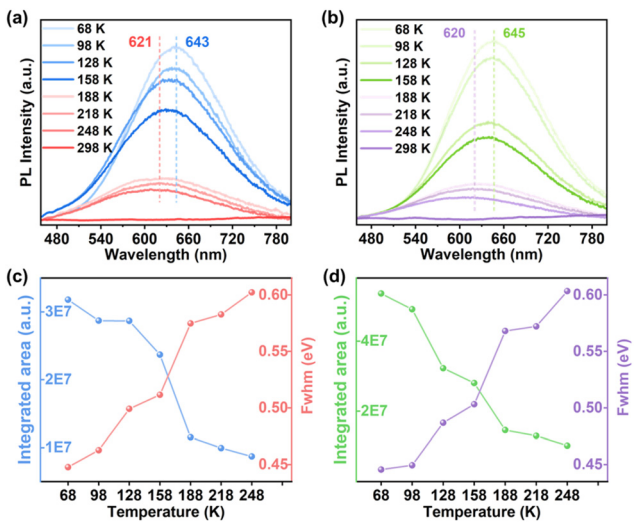

Fig. 3 Temperature-dependent PL spectra of (a) **1-CuGaS** and (b) **2-CuGaS**. PL-integrated areas and fwhm of (c) **1-CuGaS** and (d) **2-CuGaS** at different temperatures.

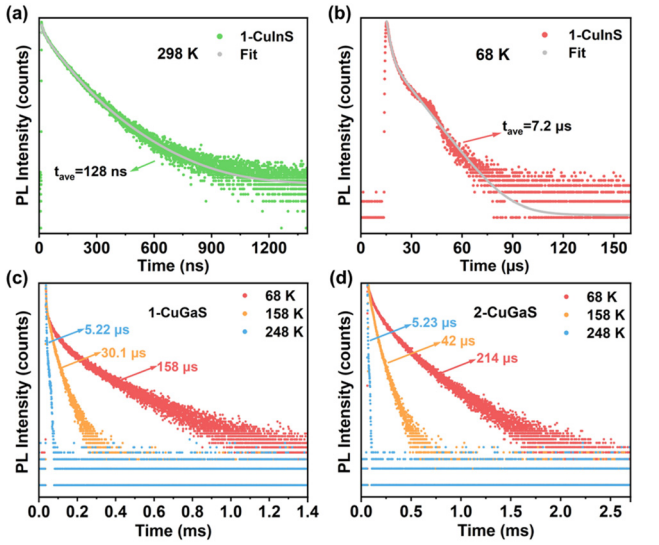

Fig. 4 PL decay curves of **1-CuInS** measured at (a) 298 K and (b) 68 K. Temperature-dependent PL decay curves of (c) **1-CuGaS** and (d) **2-CuGaS**.

increasing temperature can be attributed to the increased occurrence of non-radiative pathways.

Optical band gap and PL property of 1-CuInGaS

Based on the above results, trivalent metal ions (In^{3+} and Ga^{3+}) have indeed influence on the position of trap sites, further regulating the PL performance. To validate this hypothesis, we intentionally introduced Ga ions into **1-CuInS** and obtained **1-CuInGaS**. PXRD analysis confirmed the successful incorporation of Ga^{3+} ions into **1-CuInGaS**, causing a slight shift in peak position due to the partial replacement of In^{3+} by Ga ions (Fig. S17†). EDS data indicated that the ratio of Ga to In is about 1 : 2 in a SBU (Fig. S18†). As illustrated in Fig. 5a, **1-CuInGaS** has a band gap of 2.48 eV, which falls between the values of **1-CuInS** and **1-CuGaS**. Interestingly, under excitation of 450 nm at RT, **1-CuInGaS** exhibited dual emissions in a high-energy band (530 nm) and low-energy band (684 nm) (Fig. S19†). Notably, the high-energy band showed a blue-shift tendency with decreasing temperature, while the low-energy band displayed a red-shift tendency (Fig. 5b and S20†). Furthermore, the decay lifetime of low-energy band was much longer than that of high-energy band at both 68 K and 298 K (Fig. 5c and d; Tables S6 and S7†). In this case, the high-energy band emission in **1-CuInGaS** may result from the In^{3+} induced shallow-delocalized-traps to copper-localized hole transitions, while the low-energy band emission can be ascribed to the Ga^{3+} mediated deep-localized-traps to copper-localized hole transitions.

Optical band gap and PL property of 1-CuInCdS@*n*

With the influence of trap sites on the Cu-related emission in mind, we attempted to introduce cadmium ions to adjust the wavelength of the Cu related emission. This led to the synthesis of a series of Cd-substituted samples denoted as **1-CuInCdS@*n*** (n = 1–4). It is noted that as n increases, the ratio of Cu to Cd in these as-synthesized samples gradually increases, as illustrated by EDS measurements (Fig. S21 and Table S8†). However, cadmium ions were failed to be introduced in **1-CuGaS** and **2-CuGaS**, possibly due to the large mismatch of the atomic radius of Ga and Cd ions. PXRD analysis confirmed that **1-CuInCdS@*n*** had the same crystalline configuration with **1-CuInS** (Fig. 6a). Furthermore, UV-Vis DRS of **1-CuInCdS@*n*** were also investigated, which indicated that the addition of Cd ions to **1-CuInS** indeed led to a decrease in the position of the shallow delocalized trap sites. This decrease became more pronounced with the increase of Cu content in **1-CuInCdS@*n*** (Fig. 6b). Worth of noting is that they all exhibited the same valence band position, as confirmed by UPS (Fig. S14b†). Therefore, the shift of shallow delocalized trap sites was caused by the alteration of the conduction band position. As disclosed in Fig. 6c, **1-CuInCdS@*n*** all exhibited a redshift in PL emission compared to that of **1-CuInS**, with emission peaks at 605, 613, 624 and 633 nm, respectively, corresponding to n = 1, 2, 3, and 4. This trend in the PL performance is consistent with the red-shift of the shallow delocalized trap sites. Moreover, the temperature-dependent PLE and PL spectra of **1-CuInCdS@2** and **1-CuInCdS@4** were investigated, which showed a similar blue-shifted tendency as that of **1-CuInS** as the temperature decreased (Fig. 6d, S22, S23, and S24†). This phenomenon further illustrated that **1-CuInS** and **1-CuInCdS@*n*** had similar luminescence excitation and emission processes. PL decay dynamics of **1-CuInCdS@*n*** were also measured at 298 K (Fig. 6e and S25, and Table S2†) and at 68 K (Fig. 6f and Table S3†). All these data supported that **1-CuInS** and **1-CuInCdS@*n*** possess the same decay process. Based on the above results, we can conclude that the introduction of Cd into the framework of **1-CuInS** resulted in the redshift of the shallow-delocalized trap sites along with the emission peak.

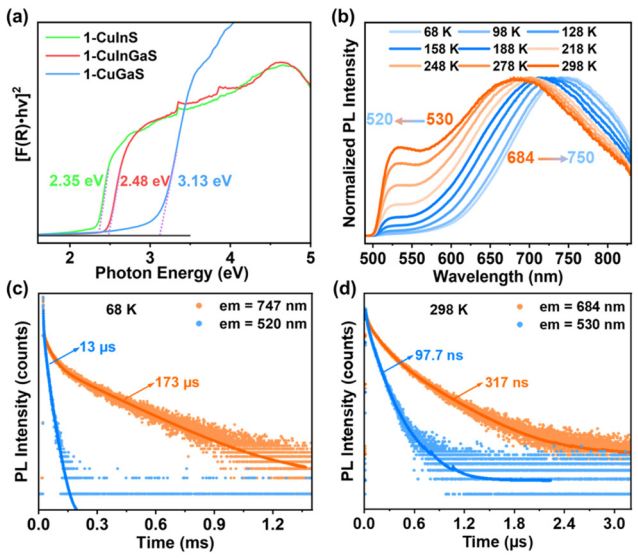

Fig. 5 (a) Tauc plots of as-synthesized **1-CuInS**, **1-CuGaS** and **1-CuInGaS**. (b) Normalized temperature-dependent PL spectra of **1-CuInGaS**. PL decay curves of the dual emission of **1-CuInGaS** at (c) 68 K and (d) 298 K.

Possible mechanism of exciton recombination

According to the above observations and previous studies, the possible mechanism of exciton recombination is depicted in Scheme 2. After absorption of light, the photo-generated electron and photo-generated hole are distributed in the conduction band (CB) and the valence band (VB), respectively. The process of radiative transition initially involves the capture of a hole from VB to the filled higher potential Cu(I) d-state, forming a transient Cu^{2+} species that contains a vacancy in the d-shell. The transient Cu^{2+} state has two different energy states, T_2 and E,[16,39,42–48] and both can accept an excited electron, which may associated with the broadening of the corresponding emission spectra. Subsequently, the green emission observed in **1-CuInS** may be assigned to the recombination of an electron in the shallow-delocalized traps with a hole in the Cu d-state. In the case of **1-CuGaS** and **2-CuGaS**, the red emission probably attributes to exciton transition from the deep-

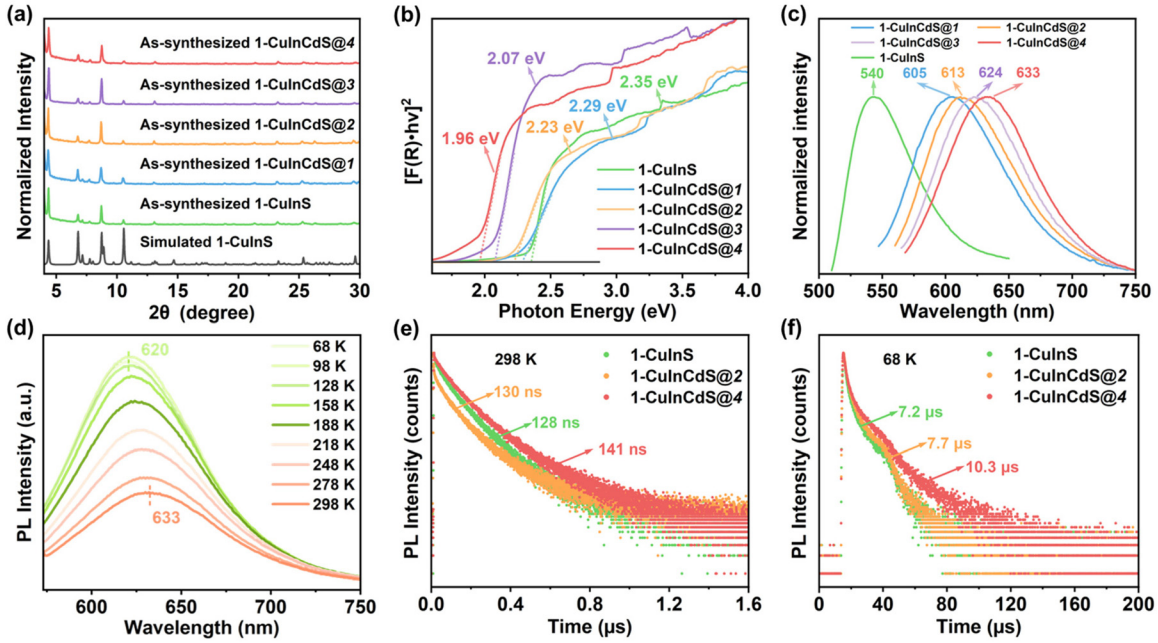

Fig. 6 (a) PXRD of simulated **1-CuInS** and as-synthesized **1-CuInS** and **1-CuInCdS@*n*** samples. (b) Tauc plots of as-synthesized **1-CuInS** and **1-CuInCdS@*n***. (c) RT PL spectra of as-synthesized **1-CuInS** and **1-CuInCdS@*n***. (d) Temperature-dependent PL spectra of **1-CuInCdS@4**. PL decay curve of as-synthesized **1-CuInS** and **1-CuInCdS@*n*** with excitation of 390 nm at (e) 298 K and (f) 68 K.

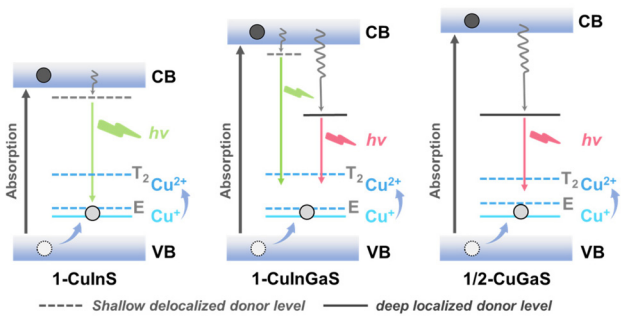

Scheme 2 Proposed energy level diagram for **1-CuInS**, **1-CuInGaS** and **1/2-CuGaS**. (VB: valence band, CB: conduction band).

localized defect state to the Cu d-state, which can be supported by the blueshift of the maximum emission wavelength with the increasing temperature and the relative longer luminescence lifetime. Furthermore, in **1-CuInGaS**, both trap sites existed simultaneously, as confirmed by the presence of green and red dual emissions. In addition, when Cd ions were introduced in **1-CuInS**, they lead to a downshift of shallow defects due to the reduction of the conduction band energy, resulting in the redshift of the emission peak of **1-CuInCdS@*n*** (Fig. S26†).

Conclusion

In summary, we for the first time systematically studied the influence of the composition-determined defect position on the luminescence in the copper-based I–III–VI metal chalcogenide nanoclusters. Three I–III–VI metal chalcogenides (**1-CuInS**, **1-CuGaS**, and **2-CuGaS**) with precise structures were selected as unique models to explore the inherent regulation mechanism of the Cu^{+}-related PL emission. Interestingly, **1-CuInS** and **1-CuGaS** with the same framework structure exhibited a large disparity in PL performance, while **1-CuGaS** and **2-CuGaS** possessing the same metal components showed similar PL property. Systematic studies shows that the green luminescence of **1-CuInS** stemmed from radiative recombination of electrons from shallow-delocalized traps to copper-localized hole and the red emission of **1-CuGaS** and **2-CuGaS** originated from radiative recombination of electrons from deep localized traps to copper-localized hole. It can conclude that the position of the traps was highly dependent on the surrounding trivalent In^{3+} and Ga^{3+} in the clusters, where the presence of In^{3+} ions will induce the formation of shallow defects and the presence of Ga^{3+} ions will produce deep defects. The deduction was further confirmed by dual emission properties of the **1-CuInGaS** with both In^{3+} and Ga^{3+} ions. Moreover, by introducing different contents of Cd ions into the **1-CuInS**, we also realized the regulation of luminescence from green emission to red emission. This work sheds light on understanding of the chemical components and defect positions relationship and the mechanism of Cu^{+}-related emission, which will stimulate further regulation of the optoelectronic properties of Cu-based nanoclusters or even nanocrystals and exploration of their potential applications.

Author contributions

Tao Wu and Shang-Fu Yuan: funding acquisition, project administration, resources, writing – reviewing, editing and supervision. Dong-Sheng Li: funding acquisition. Rui Zhou: funding acquisition. Yi-Lei Xu and Yayun Ding: conceptualization, data curation, formal analysis, investigation, methodology, writing – reviewing and editing. Lin-Mei Zhang, Hao Ma, Jia-Xing Liu and Jiaxu Zhang: formal analysis.

Conflicts of interest

There are no conflicts to declare.

Acknowledgements

We acknowledge National Natural Science Foundation of China (22071165, 92261205, 22201103, and U22A20432) and the 111 Project (D20015).

References

1 R. Xie, M. Rutherford and X. Peng, Formation of High-Quality I–III–VI Semiconductor Nanocrystals by Tuning Relative Reactivity of Cationic Precursors, *J. Am. Chem. Soc.*, 2009, **131**, 5691–5697.
2 H. Zhong, Z. Bai and B. Zou, Tuning the Luminescence Properties of Colloidal I–III–VI Semiconductor Nanocrystals for Optoelectronics and Biotechnology Applications, *J. Phys. Chem. Lett.*, 2012, **3**, 3167–3175.
3 C. Guillén, $CuInS_2$ thin films grown sequentially from binary sulfides as compared to layers evaporated directly from the elements, *Semicond. Sci. Technol.*, 2006, **21**, 709–712.
4 Y.-K. Kim, S.-H. Ahn, K. Chung, Y.-S. Cho and C.-J. Choi, The photoluminescence of $CuInS_2$ nanocrystals: effect of non-stoichiometry and surface modification, *J. Mater. Chem.*, 2011, **22**, 1516–1520.
5 H. Nakamura, W. Kato, M. Uehara, K. Nose, T. Omata, S. Otsuka-Yao-Matsuo, M. Miyazaki and H. Maeda, Tunable Photoluminescence Wavelength of Chalcopyrite $CuInS_2$-Based Semiconductor Nanocrystals Synthesized in a Colloidal System, *Chem. Mater.*, 2006, **18**, 3330–3335.
6 T. Omata, K. Nose and S. Otsuka-Yao-Matsuo, Size dependent optical band gap of ternary I-III-VI_2 semiconductor nanocrystals, *J. Appl. Phys.*, 2009, **105**, 073106.
7 Y.-B. Shan, X.-F. Yue, J.-J. Chen, J.-K. Han, G. Ekoya, L.-G. Hu, R. Liu, Z.-J. Qiu and C.-X. Cong, Revealing layer-dependent interlayer interactions by doping effect on graphene in WSe_2/N-layer graphene heterostructures using Raman and photoluminescence spectroscopy, *Rare Met.*, 2022, **41**, 3646–3653.
8 Z.-W. Zhang, Q.-H. Li, X.-Q. Qiao, D. Hou and D.-S. Li, One-pot hydrothermal synthesis of willow branch-shaped MoS_2/CdS heterojunctions for photocatalytic H_2 production under visible light irradiation, *Chin. J. Catal.*, 2019, **40**, 371–379.
9 F.-Y. Tian, D. Hou, F. Tang, M. Deng, X.-q. Qiao, Q. Zhang, T. Wu and D.-S. Li, Novel $Zn_{0.8}Cd_{0.2}S$@g-C_3N_4 core–shell heterojunctions with a twin structure for enhanced visible-light-driven photocatalytic hydrogen generation, *J. Mater. Chem. A*, 2018, **6**, 17086–17094.
10 M. Jiao, X. Huang, L. Ma, Y. Li, P. Zhang, X. Wei, L. Jing, X. Luo, A. L. Rogach and M. Gao, Biocompatible off-stoichiometric copper indium sulfide quantum dots with tunable near-infrared emission via aqueous based synthesis, *Chem. Commun.*, 2019, **55**, 15053–15056.
11 S. H. Park, A. Hong, J.-H. Kim, H. Yang, K. Lee and H. S. Jang, Highly Bright Yellow-Green-Emitting $CuInS_2$ Colloidal Quantum Dots with Core/Shell/Shell Architecture for White Light-Emitting Diodes, *ACS Appl. Mater. Interfaces*, 2015, **7**, 6764–6771.
12 H. C. Yoon, J. H. Oh, M. Ko, H. Yoo and Y. R. Do, Synthesis and Characterization of Green Zn–Ag–In–S and Red Zn–Cu–In–S Quantum Dots for Ultrahigh Color Quality of Down-Converted White LEDs, *ACS Appl. Mater. Interfaces*, 2015, **7**, 7342–7350.
13 C.-W. Chen, D.-Y. Wu, Y.-C. Chan, C. C. Lin, P.-H. Chung, M. Hsiao and R.-S. Liu, Evaluations of the Chemical Stability and Cytotoxicity of $CuInS_2$ and $CuInS_2$/ZnS Core/Shell Quantum Dots, *J. Phys. Chem. C*, 2015, **119**, 2852–2860.
14 W. Guo, X. Sun, O. Jacobson, X. Yan, K. Min, A. Srivatsan, G. Niu, D. O. Kiesewetter, J. Chang and X. Chen, Intrinsically Radioactive [^{64}Cu]CuInS/ZnS Quantum Dots for PET and Optical Imaging: Improved Radiochemical Stability and Controllable Cerenkov Luminescence, *ACS Nano*, 2015, **9**, 488–495.
15 A. C. Berends, F. T. Rabouw, F. C. M. Spoor, E. Bladt, F. C. Grozema, A. J. Houtepen, L. D. A. Siebbeles and C. de Mello Donegá, Radiative and Nonradiative Recombination in $CuInS_2$ Nanocrystals and $CuInS_2$-Based Core/Shell Nanocrystals, *J. Phys. Chem. Lett.*, 2016, **7**, 3503–3509.
16 K. E. Knowles, K. H. Hartstein, T. B. Kilburn, A. Marchioro, H. D. Nelson, P. J. Whitham and D. R. Gamelin, Luminescent Colloidal Semiconductor Nanocrystals Containing Copper: Synthesis, Photophysics, and Applications, *Chem. Rev.*, 2016, **116**, 10820–10851.
17 T. Uematsu, T. Doi, T. Torimoto and S. Kuwabata, Preparation of Luminescent $AgInS_2$–$AgGaS_2$ Solid Solution Nanoparticles and Their Optical Properties, *J. Phys. Chem. Lett.*, 2010, **1**, 3283–3287.
18 M. Uehara, K. Watanabe, Y. Tajiri, H. Nakamura and H. Maeda, Synthesis of $CuInS_2$ fluorescent nanocrystals and enhancement of fluorescence by controlling crystal defect, *J. Chem. Phys.*, 2008, **129**, 134709.
19 J. Zhang, P. Feng, X. Bu and T. Wu, Atomically precise metal chalcogenide supertetrahedral clusters: frameworks to molecules, and structure to function, *Natl. Sci. Rev.*, 2021, **9**, nwab076.
20 J. Wu, B. Jin, X. Wang, Y. Ding, X.-L. Wang, D. Tang, X. Li, J. Shu, D.-S. Li, Q. Lin, Y.-B. Wu and T. Wu, Breakdown of

Valence Shell Electron Pair Repulsion Theory in an H-Bond-Stabilized Linear sp-Hybridized Sulfur, *CCS Chem.*, 2021, **3**, 2584–2590.

21 J. Zhang, X. Bu, P. Feng and T. Wu, Metal Chalcogenide Supertetrahedral Clusters: Synthetic Control over Assembly, Dispersibility, and Their Functional Applications, *Acc. Chem. Res.*, 2020, **53**, 2261–2272.

22 J. Lin, Q. Zhang, L. Wang, X. Liu, W. Yan, T. Wu, X. Bu and P. Feng, Atomically Precise Doping of Monomanganese Ion into Coreless Supertetrahedral Chalcogenide Nanocluster Inducing Unusual Red Shift in Mn^{2+} Emission, *J. Am. Chem. Soc.*, 2014, **136**, 4769–4779.

23 N. Zheng, X. Bu, B. Wang and P. Feng, Microporous and Photoluminescent Chalcogenide Zeolite Analogs, *Science*, 2002, **298**, 2366–2369.

24 J. Lin, L. Wang, Q. Zhang, F. Bu, T. Wu, X. Bu and P. Feng, Highly effective nanosegregation of dual dopants in a micron-sized nanocluster-based semiconductor molecular single crystal for targeting white-light emission, *J. Mater. Chem. C*, 2016, **4**, 1645–1650.

25 H. Yang, J. Zhang, M. Luo, W. Wang, H. Lin, Y. Li, D. Li, P. Feng and T. Wu, The Largest Supertetrahedral Oxychalcogenide Nanocluster and Its Unique Assembly, *J. Am. Chem. Soc.*, 2018, **140**, 11189–11192.

26 J. Zhang, C. Qin, Y. Zhong, X. Wang, W. Wang, D. Hu, X. Liu, C. Xue, R. Zhou, L. Shen, Y. Song, D. Xu, Z. Lin, J. Guo, H. Su, D.-S. Li and T. Wu, Atomically precise metal-chalcogenide semiconductor molecular nanoclusters with high dispersibility: Designed synthesis and intracluster photocarrier dynamics, *Nano Res.*, 2020, **13**, 2828–2836.

27 Y. Hou, T. Wu, L. Wang and P. Feng, Integration of supertetrahedral cluster with reduced graphene oxide sheets for enhanced photostability and photoelectrochemical properties, *Sci. China: Chem.*, 2013, **56**, 423–427.

28 X. Xu, D. Hu, C. Xue, J. Zhang, D.-S. Li and T. Wu, Exploring the effects of intercluster torsion stress on Mn^{2+}-related red emission from cluster-based layered metal chalcogenides, *J. Mater. Chem. C*, 2018, **6**, 10480–10485.

29 J. Lin, D.-D. Hu, Q. Zhang, D.-S. Li, T. Wu, X. Bu and P. Feng, Improving Photoluminescence Emission Efficiency of Nanocluster-Based Materials by in Situ Doping Synthetic Strategy, *J. Mater. Chem. C*, 2016, **120**, 29390–29396.

30 Y. Liu, J. Zhang, B. Han, X. Wang, Z. Wang, C. Xue, G. Bian, D. Hu, R. Zhou, D.-S. Li, Z. Wang, Z. Ouyang, M. Li and T. Wu, New Insights into Mn–Mn Coupling Interaction-Directed Photoluminescence Quenching Mechanism in Mn^{2+}-Doped Semiconductors, *J. Am. Chem. Soc.*, 2020, **142**, 6649–6660.

31 X. Bu, N. Zheng, Y. Li and P. Feng, Pushing Up the Size Limit of Chalcogenide Supertetrahedral Clusters: Two- and Three-Dimensional Photoluminescent Open Frameworks from $(Cu_5In_{30}S_{54})^{13-}$ Clusters, *J. Am. Chem. Soc.*, 2002, **124**, 12646–12647.

32 Z.-Q. Li, C.-J. Mo, Y. Guo, N.-N. Xu, Q.-Y. Zhu and J. Dai, Discrete supertetrahedral CuInS nanoclusters and their application in fabrication of cluster-sensitized TiO_2 photoelectrodes, *J. Mater. Chem. A*, 2017, **5**, 8519–8525.

33 W.-W. Xiong, J.-R. Li, B. Hu, B. Tan, R.-F. Li and X.-Y. Huang, Largest discrete supertetrahedral clusters synthesized in ionic liquids, *Chem. Sci.*, 2012, **3**, 1200–1204.

34 D.-D. Yang, W. Li, W.-W. Xiong, J.-R. Li and X.-Y. Huang, Ionothermal synthesis of discrete supertetrahedral Tn (n = 4, 5) clusters with tunable components, band gaps, and fluorescence properties, *Dalton Trans.*, 2018, **47**, 5977–5984.

35 A. A. Bol, J. Ferwerda, J. A. Bergwerff and A. Meijerink, 26-Luminescence of nanocrystalline ZnS:Cu^{2+}, *J. Lumin.*, 2002, **99**, 325–334.

36 S. M. Thompson, C. Şahin, S. Yang, M. E. Flatté, C. B. Murray, L. C. Bassett and C. R. Kagan, Red Emission from Copper-Vacancy Color Centers in Zinc Sulfide Colloidal Nanocrystals, *ACS Nano*, 2023, **17**, 5963–5973.

37 Y. P. Varshni, Temperature dependence of the energy gap in semiconductors, *Physica*, 1967, **34**, 149–154.

38 J. F. Suyver, T. van der Beek, S. F. Wuister, J. J. Kelly and A. Meijerink, Luminescence of nanocrystalline ZnSe:Cu, *Appl. Phys. Lett.*, 2001, **79**, 4222–4224.

39 P. Peka and H.-J. Schulz, Empirical one-electron model of optical transitions in Cu-doped ZnS and CdS, *Phys. B*, 1994, **193**, 57–65.

40 S. Shionoya, T. Koda, K. Era and H. Fujiwara, Nature of Luminescence Transitions in ZnS Crvstals, *J. Phys. Soc. Jpn.*, 1964, **19**, 1157–1167.

41 P. Mondal and R. Viswanatha, Insights into the Oxidation State of Cu Dopants in II–VI Semiconductor Nanocrystals, *J. Phys. Chem. Lett.*, 2022, **13**, 1952–1961.

42 J. L. Birman, Electronic Structure of the Centers in ZnS, *Phys. Rev.*, 1961, **121**, 144–145.

43 P. Peka and H.-J. Schulz, Unified description of Cu-related luminescence processes in II–VI semiconductors, *Solid State Commun.*, 1994, **89**, 225–228.

44 S. Gul, J. K. Cooper, C. Corrado, B. Vollbrecht, F. Bridges, J. Guo and J. Z. Zhang, Synthesis, Optical and Structural Properties, and Charge Carrier Dynamics of Cu-Doped ZnSe Nanocrystals, *J. Phys. Chem. C*, 2011, **115**, 20864–20875.

45 B. B. Srivastava, S. Jana and N. Pradhan, Doping Cu in Semiconductor Nanocrystals: Some Old and Some New Physical Insights, *J. Am. Chem. Soc.*, 2011, **133**, 1007–1015.

46 H. D. Nelson, X. Li and D. R. Gamelin, Computational Studies of the Electronic Structures of Copper-Doped CdSe Nanocrystals: Oxidation States, Jahn–Teller Distortions, Vibronic Bandshapes, and Singlet–Triplet Splittings, *J. Phys. Chem. C*, 2016, **120**, 5714–5723.

47 J. K. Cooper, S. Gul, S. A. Lindley, J. Yano and J. Z. Zhang, Tunable Photoluminescent Core/Shell Cu^{+}-Doped ZnSe/ZnS Quantum Dots Codoped with Al^{3+}, Ga^{3+}, or In^{3+}, *ACS Appl. Mater. Interfaces*, 2015, **7**, 10055–10066.

48 S. Gul, J. K. Cooper, P.-A. Glans, J. Guo, V. K. Yachandra, J. Yano and J. Z. Zhang, Effect of Al^{3+} Co-doping on the Dopant Local Structure, Optical Properties, and Exciton Dynamics in Cu^{+}-Doped ZnSe Nanocrystals, *ACS Nano*, 2013, **7**, 8680–8692.

